PHYSICAL REVIEW B **90**, 085118 (2014)

Effects of van der Waals interactions and quasiparticle corrections on the electronic and transport properties of Bi_2Te_3

L. Cheng,[1] H. J. Liu,[1,*] J. Zhang,[1] J. Wei,[1] J. H. Liang,[1] J. Shi,[1] and X. F. Tang[2]
[1]*Key Laboratory of Artificial Micro- and Nano-Structures of Ministry of Education and School of Physics and Technology, Wuhan University, Wuhan 430072, China*
[2]*State Key Laboratory of Advanced Technology for Materials Synthesis and Processing, Wuhan University of Technology, Wuhan 430070, China*

(Received 21 May 2014; revised manuscript received 27 July 2014; published 14 August 2014)

We present a theoretical study of the structural, electronic, and transport properties of bulk Bi_2Te_3 within density functional theory taking into account the van der Waals interactions (vdW) and the quasiparticle self-energy corrections. It is found that the optB86b-vdW functional can well reproduce the experimental lattice constants and interlayer distances for Bi_2Te_3. Based on the fully optimized structure, the band structure of Bi_2Te_3 is obtained from first-principles calculations with the *GW* approximation and the Wannier function interpolation method. The global band extrema are found to be off the high-symmetry lines, and the real energy band calculated is in good agreement with that measured experimentally. In combination with the Boltzmann theory, the *GW* calculations also give accurate prediction of the transport properties, and the calculated thermoelectric coefficients of Bi_2Te_3 almost coincide with the experimental data.

DOI: 10.1103/PhysRevB.90.085118 PACS number(s): 72.15.Jf, 71.15.Mb, 71.20.Nr

I. INTRODUCTION

As a traditional good thermoelectric material, bismuth telluride has attracted lots of experimental and theoretical investigations on the electronic and transport properties. Bulk Bi_2Te_3 has a rhombohedral structure belonging to the space group $R\bar{3}m$ with five atoms in the unit cell (Fig. 1). They form stacks of covalently bonded quintuple layers (QLs) in the sequence of Te1-Bi-Te2-Bi-Te1, where the QLs are bounded through weak van der Waals (vdW) interactions. Unfortunately, the traditional density functional theory (DFT) is unable to account for long range vdW interactions. Although vdW interaction is usually very weak, it can have a significant effect on the inter-QL distance [1] which in turn may play an important role in determining the electronic and transport properties of bulk Bi_2Te_3. Recently, Grimme proposed the D2 method by adding a correction to the conventional Kohn-Sham DFT energy to treat the vdW interactions [2]. Dion *et al.* [3] proposed a nonlocal correlation functional which approximately accounts for the dispersion interactions. The so-called vdW-DF is implemented into DFT to deal with the weak vdW interactions [4]. Cooper reported an exchange functional that is compatible with the Rutgers-Chalmers vdW correlation functional [5]. Luo *et al.* [1] investigated the atomic, electronic, and thermoelectric properties of bulk Bi_2Te_3 and Bi_2Se_3 with the vdW interactions included, and they found that using the vdW-DF_x^{C09} functional (means C09 exchange) gives a much better agreement with the experimental structural parameters. Moreover, their calculations indicated that vdW interactions are crucial for the electronic and thermoelectric properties. Liu *et al.* [6] considered few QLs films of Bi_2Te_3 and Bi_2Se_3, and found that the vdW interactions are needed to obtain correct lattice parameters and energy band structures.

Recently, Bi_2Te_3 has been subject to extensive study not only as a good thermoelectric material, but also as a good topological insulator (TI) [7–9]. The theoretical study of TIs involves very precise electronic calculations for the excited-state properties, which is beyond the scope of traditional DFT. One approach to overcome this deficiency is to calculate the quasiparticle properties with the *GW* approximation of the many-body effects [10,11]. In fact, the *GW* method has been applied to study the electronic structures of Bi_2Te_3 in several previous reports [12–15]. In Ref. [12] Kioupakis *et al.* calculated the quasiparticle band structures of Bi_2Te_3 with the experimental lattice parameter and found that it has direct and indirect band gaps that are very close to each other (~0.17 eV). In Ref. [14] Nechaev and Chulkov showed how the atomic positions, the DFT exchange correlation functionals, and the *GW* approximation affect the location of band extrema and thus the band gap of Bi_2Te_3. They found that the GGA+*GW* with relaxed atomic positions gives a band gap of 156 meV, which agrees well with the experimental value. The conduction band minimum (CBM) and the valance band maximum (VBM) they found is similar to those appearing in angle resolved photoemission spectroscopy (ARPES) measurements [16].

Although extensive electronic structures and transport calculations have been performed for Bi_2Te_3, however, most of them are calculated using the experimental structural parameters without full relaxations in a self-consistent way. There are also theoretical works taking into account the vdW interactions [1,6], or including the *GW* approximation [12–15]. However, to the best of our knowledge, no work has been reported so far considering both of them, especially for their combined effects on the electronic and transport properties of Bi_2Te_3. In the present work we first optimize the atomic structure of Bi_2Te_3 by using appropriate vdW functionals. We next calculate the electronic structure of Bi_2Te_3 with the vdW interactions and *GW* approximation both considered. The transport properties are then derived by a combination of Boltzmann theory and Wannier interpolation method. The thermoelectric transport properties of Bi_2Te_3 predicted from our theoretical calculations are in excellent agreement with those measured experimentally.

---

[*] Author to whom correspondence should be addressed: phlhj@whu.edu.cn

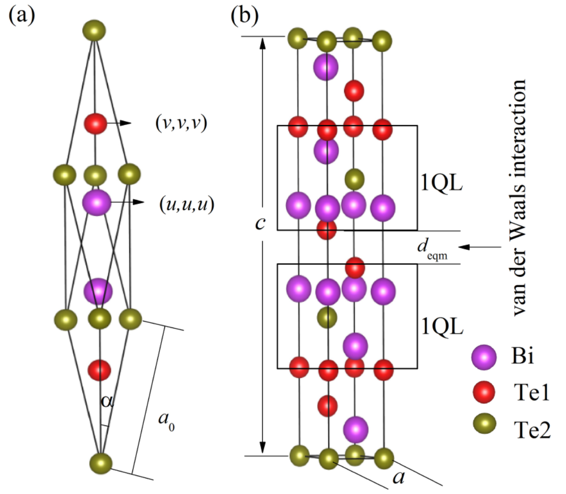

FIG. 1. (Color online) The crystal structure of Bi_2Te_3 showing (a) rhombohedral unit cell and (b) hexagonal unit cell.

II. COMPUTATIONAL DETAILS

Our theoretical calculations have been performed by using the projector augmented-wave method [17,18] within the framework of DFT [19–21]. The exchange correlation energy is in the form of Perdew-Burke-Ernzerhof [22] with generalized gradient approximation (GGA). For structural optimization, the energy cutoff is set as 400 eV and the Brillouin zone is sampled with $9 \times 9 \times 9$ Monkhorst-Pack $\boldsymbol{k}$ meshes. Optima atom positions are determined until the magnitude of the force acting on each Bi atom becomes less than 0.01 eV/Å. In order to illustrate the vdW interactions effects on the lattice parameters, a detailed investigation with different forms of vdW exchange correlation functionals have been performed. For the *GW* calculation, we use a partially self-consistent GW_0 in the present work, which means that our results are obtained by iterating only G, but keeping W fixed to the initial DFT W_0. The spin-orbit coupling effects are included which is fully relativistic for the core electrons and using the second-variation method for the valence states [23]. The Brillouin zone is sampled with $6 \times 6 \times 6$ Γ centered grids. The static dielectric function was evaluated with a sum over 272 unoccupied bands. For the maximally localized Wannier function generation process, we started with an initial guess of one s and three p orbits per atom, and used the disentanglement technique to extract 40 Wannier functions. The electronic structures are then obtained using the Wannier interpolation formalism [24–26]. To locate the exact VBM and CBM and thus the real band gap, a very dense $\boldsymbol{k}$ meshing up to 4960 points is used in the irreducible Brillouin zone. The electronic transport properties are computed using the semiclassical Boltzmann theory with the maximally localized Wannier function basis to interpolate band structures and band velocities [27].

III. RESULTS AND DISCUSSIONS

A. Structural properties of Bi_2Te_3 including vdW interactions

The crystal structure of Bi_2Te_3 is shown in Fig. 1. The experimentally measured lattice parameters are $a_0 = 10.476$ Å and $\alpha = 24.166°$ [28], which corresponds to $a = 4.386$ Å and $c = 30.497$ Å in a hexagonal cell. The internal coordinates are $u = 0.4000$ for a Bi atom and $v = 0.2095$ for a Te1 atom, and the inter-QL distance is $d_{\mathrm{eqm}} = 2.612$ Å. On the theoretical side, extensive DFT calculations [29–34] have been performed for bulk Bi_2Te_3. However, most of them deal with the experimental lattice parameters, and their calculations do not properly treat the long-range dispersion interactions. There is currently growing interest in the calculations with vdW interactions explicitly implemented, and various kinds of vdW functionals have been suggested [2–4,35,36]. In principle, these vdW functionals can be classified into two kinds: The first is to add a correction to the conventional Kohn-Sham DFT energy (DFT-D2 or DFT-D3) [2], and the second is a nonlocal correlation functional that approximately accounts for dispersion interactions (vdW-DF). In practice, several variants of the vdW-DF were proposed: the original “vdW-DF” [3], the “opt” functionals (optPBE-vdW, optB88-vdW, and optB86b-vdW) [35], and the “vdW-DF2” [36]. All of them have nonlocal correlation functionals (Langreth-Lundqvist style) [4] that approximately account for dispersion interactions, but with slightly different exchange functionals. Using these functionals, we calculate the structural parameters of Bi_2Te_3 and our results are summarized in Table I. The experiment results are also given for comparison. It is obvious that the standard DFT with PBE functional tends to overestimate the lattice parameters. Such overestimation will be reduced more or less when the vdW

TABLE I. Structural parameters of bulk Bi_2Te_3 calculated with various kinds of vdW functionals. Here a_0 and α correspond to the rhombohedral cell, while a and c correspond to hexagonal cell. u and v are the internal coordinates of Bi and Te1 atoms in terms of ($\pm u$, $\pm u$, $\pm u$) and ($\pm v$, $\pm v$, $\pm v$), respectively. d_{eqm} is the equilibrium inter-QL distance. The experimental results from Ref. [28] are also listed for comparison.

	Expt.	PBE	DFT-D2	optB86b -vdW	optB88 -vdW	optPBE -vdW	vdW-DF2
a_0 (Å)	10.476	10.970	10.747	10.570	10.697	10.889	11.148
α (deg)	24.166	23.351	23.226	24.075	23.975	24.650	23.866
u (Bi)	0.4000	0.3974	0.3984	0.3995	0.3992	0.3984	0.3988
v (Te)	0.2095	0.2153	0.2122	0.2106	0.2118	0.2135	0.2141
a (Å)	4.386	4.440	4.327	4.409	4.443	4.463	4.610
c (Å)	30.497	31.998	31.357	30.778	31.153	31.741	32.477
d_{eqm}(Å)	2.612	3.112	2.855	2.704	2.812	2.973	3.081

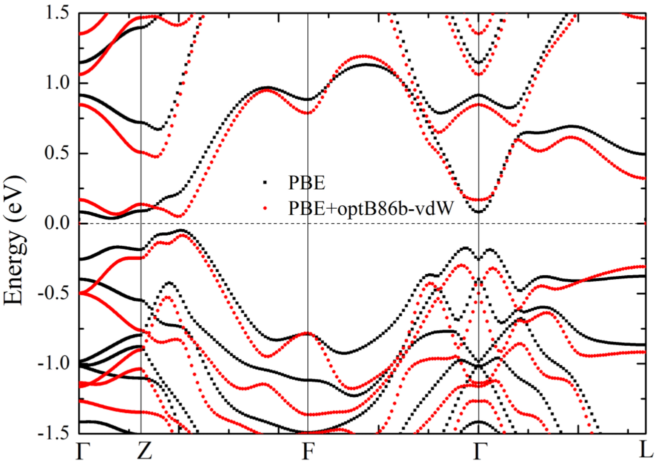

FIG. 2. (Color online) Calculated energy band structures of Bi_2Te_3. The black and red lines correspond to the calculations with PBE and PBE+optB86b-vdW, respectively. The Fermi level is at 0 eV.

interactions are considered in the calculations. This observation holds for all the mentioned vdW functionals except for the vdW-DF2 functional. It should be mentioned that a_0 and c calculated with vdW-DF2 are very close to that predicted using $\mathrm{vdW} - \mathrm{DF}_x^{\mathrm{revPBE}}$ functional (means revPBE exchange) [1]. For all the investigated functionals, the difference in the internal coordinates is very small, which is consistent with that found in Ref. [1]. As for the inter-QL distance d_{eqm} which is closely related to the vdW interactions, we see from Table I that the standard PBE functional predicts a value of 3.112 Å, which is larger than that measured experimentally by about 19%. Such a bigger difference suggests that the vdW interactions cannot be ignored when dealing with the physical properties of Bi_2Te_3 and similar structures. We further find that the calculation with the optB86b-vdW functional gives a d_{eqm} value of 2.704 Å, which is in better agreement with the experimental value of 2.612 Å. Among all the discussed vdW functionals, the ability of the optB86b-vdW functional in predicting the lattice structure of Bi_2Te_3 is the best, and is thus used exclusively in our following calculations.

B. Electronic properties of Bi_2Te_3 with PBE+optB86b-vdW functional

The importance of appropriate treatment of vdW interactions lies not only in accurately predicting the structural parameters of Bi_2Te_3, but also the electronic properties. Figure 2 displays the energy band structures of Bi_2Te_3 along several high symmetry lines in the irreduced Brillouin zone. For comparison, the calculations with standard PBE and PBE+optB86b-vdW are both shown. Indeed, we see the vdW has real effect on the energy band structure and obvious differences in the band shape and band gap are observed. In particular, we find that including vdW leads to an extra degeneracy of the top two valence bands at the Γ point, which is believed to be caused by a decrease of inter-QL distance d_{eqm} (from 3.112 to 2.704 Å). Further decrease of d_{eqm} can lead to a band crossing near the Γ point [1]. On the other hand, the band gaps calculated with and without vdW interactions are 134 and 85 meV, respectively. It seems that the former agrees well with the experimentally measured gap of 150 ± 20 meV [37–39]. However, such coincidence is actually questionable since it is well known that DFT usually underestimates the band gap seriously. A careful search in the Brillouin zone using very dense $\boldsymbol{k}$ mesh indicates that the CBM and VBM actually do not locate at those high-symmetry lines shown in Fig. 2. For the PBE+optB86b-vdW, the VBM and CBM appear at $\boldsymbol{k}$ points (0.553, 0.395, 0.395) and (0.658, 0.553, 0.553) of the Brillouin zone (given in reduced coordinates in the rhombohedral cell). The energy difference between these two points should be regarded as the real band gap, which is calculated to be 108 meV. Our calculated results are summarized in Table II together with previous theoretical findings. It should be mentioned that the band extrema we obtained are very close to those found in Refs. [40] and [41]. Note in some of these works [12,40–42,45], the lattice parameters used for band structure calculations are directly taken from the experimental data.

C. Electronic properties of Bi_2Te_3 with PBE+optB86b-vdW+GW

As mentioned above, the band gap of Bi_2Te_3 calculated with PBE+optB86b-vdW is still smaller than the experimental value. This is a known limitation of DFT which can be

TABLE II. The locations of VBM and CBM as well as the corresponding band gap of bulk Bi_2Te_3, calculated with and without GW approximations. The results from previous calculations are also listed.

Reference without *GW*	VBM	CBM	Gap (eV)
Youn and Freeman [40]	(0.546, 0.383, 0.383)	(0.663, 0.568, 0.568)	0.06
Larson [42]	(0.546, 0.383, 0.383)	(0.381, 0.500, 0.500)	0.05
Scheidemantel *et al.* [45]	(0.652, 0.579, 0.579)	(0.663, 0.568, 0.568)	0.11
Kim *et al.* [41]	(0.646, 0.549, 0.549)	(0.555, 0.397, 0.394)	0.154
Wang and Cagin [32]	(0.662, 0.584, 0.584)	(0.673, 0.579, 0.579)	0.049
Kioupakis *et al.* [12]	(0.37, 0.54, 0.37)	(0.58, 0.68, 0.58)	0.087
This study	(0.553, 0.395, 0.395)	(0.658, 0.553, 0.553)	0.108
Reference with *GW*	VBM	CBM	Gap (eV)
Kioupakis *et al.* [12]	(0.66, 0.58, 0.58)	(0.67, 0.58, 0.58)	0.165
This study	(0.639, 0.560, 0.560)	(0.658, 0.579, 0.579)	0.157

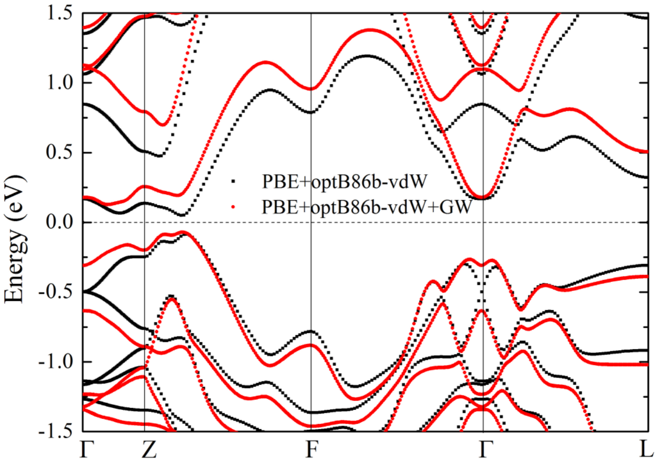

FIG. 3. (Color online) Calculated energy band structures of Bi_2Te_3. The black and red lines correspond to the calculations with PBE+optB86b-vdW and PBE+optB86b-vdW+*GW*, respectively. The Fermi level is at 0 eV.

essentially solved by performing the *GW* calculations. The *GW* method could accurately predict the excited-state properties, such as the band gaps and quasiparticle energies, although more computational efforts are required. Figure 3 shows the *GW* calculated energy band structures of Bi_2Te_3. Note here the vdW functional in the form of optB86b is by default included in the calculations. For comparison, the result without *GW* is also shown. There are some noticeable differences between these two band structures. First, in the case of PBE+optB86b-vdW calculations, the VBM and CBM observed from the band structure (not necessarily the real ones) are both located in the *Z*-*F* direction; while the *GW* predicted VBM and CBM appear in the *Z*-*F* and Γ-*Z* directions, respectively. As a result, the gap between them increases from 134 to 197 meV when the *GW* correction is applied. Second, the DFT calculated band gap at the Γ point (0.68 eV) is larger than that of the *GW* calculation (0.49 eV). Third, the *camelback* shape of the highest valance band around the Γ point turns to be flattened when the *GW* approximation is taken into account. Finally, the *GW* tends to downshift the valance bands but upshift the conduction bands. Our calculated band structure agrees well with those found in previous works using different *GW* codes such as *SPEX* [14,15] and *BERKELEYGW* [13], which further confirms the reliability of our approach (see details in the Supplemental Material [46]).

It should be emphasized that the VBM and CBM of Bi_2Te_3 obtained directly from the energy band structure may not be the global band extrema. We thus perform an entire search of the Brillouin zone and the real VBM and CBM are found to be located at ***k*** points of (0.639, 0.560, 0.560) and (0.658, 0.579, 0.579), respectively. The real energy gap with *GW* corrections is thus calculated to be 157 meV, which is in excellent agreement with the experimental value [37–39]. Note the locations of VBM and CBM and the gap value in the present work are very close to those found in Ref. [12]. Our *GW* calculated results are also summarized in Table II.

Up to now we become aware of the importance of the vdW interactions and quasiparticle corrections. Only when both effects are appropriately taken into consideration can we give an accurate prediction of the structural and electronic properties of Bi_2Te_3. There is no doubt that such effects will also play an important role in determining the transport properties of Bi_2Te_3, which will be discussed in the following section.

D. Transport properties of Bi_2Te_3 with *GW* approximation

As a traditional good thermoelectric material, the electronic transport properties of Bi_2Te_3 have been widely investigated. By using the Boltzmann theory and relaxation time approximation, the Seebeck coefficient S, the electrical conductivity σ, and the electronic thermal conductivity κ_e can be essentially derived [41,42,45]. However, most of such kinds of calculations are performed without considering the *GW* approximation, and there is usually an underestimation of the Seebeck coefficients. To address this problem, here the Boltzmann transport theory is combined with the maximally localized Wannier function basis to interpolate the band structures and band velocities. To incorporate the temperature dependence of the band structures, we assume that the band shape does not change with temperature, but shift the valence or conduction bands which gives a temperature-dependent band gap $\Delta E_g = (0.157 - 1.08 \times 10^{-4}T)$ eV [37,38,43].

Pristine Bi_2Te_3 is known to exhibit p-type intrinsic conduction below room temperatures and the saturation hole concentration is found to be 1.1×10^{19} cm^{-3} [43]. In Table III we list a series of experimentally measured hole concentrations at temperature ranging from 100 to 500 K [43]. At these particular concentrations, the calculated in-plane Seebeck coefficient S as a function of temperature is plotted in Fig. 4(a). The experimentally measured values [43] are also shown as a comparison. For p-type conduction we see that the Seebeck coefficients calculated with *GW* involved agree well with the experimental results below 300 K. At temperature above 300 K, however, the *GW* calculated results are much larger than those found experimentally. The observed rapid decrease of Seebeck coefficients can be explained as that more n-type carriers are excited at higher temperature. To clarify this

TABLE III. The fitted relaxation time of bulk Bi_2Te_3 at a series of temperature. Here n_p and σ_{exp} are, respectively, the hole concentration and electrical conductivity measured in Ref. [43]. σ/τ is the calculated electrical conductivity with respect to the relaxation time τ.

Temperature (K)	100	150	200	250	300	350	400	450	500
n_p (10^{19}/cm^3)	1.1	1.1	1.1	1.1	1.1	1.6	1.7	2.0	2.5
σ_{exp} ($10^4\Omega^{-1}$ m^{-1})	38.5	22.5	12	7.5	5.0	4.9	5.0	5.5	7.5
σ/τ ($10^3\Omega^{-1}$ m^{-1} fs^{-1})	3.77	4.17	4.55	4.73	4.73	5.82	6.36	7.13	7.54
τ (10^{-14} s)	10.2	5.39	2.64	1.58	1.06	0.84	0.79	0.77	0.99

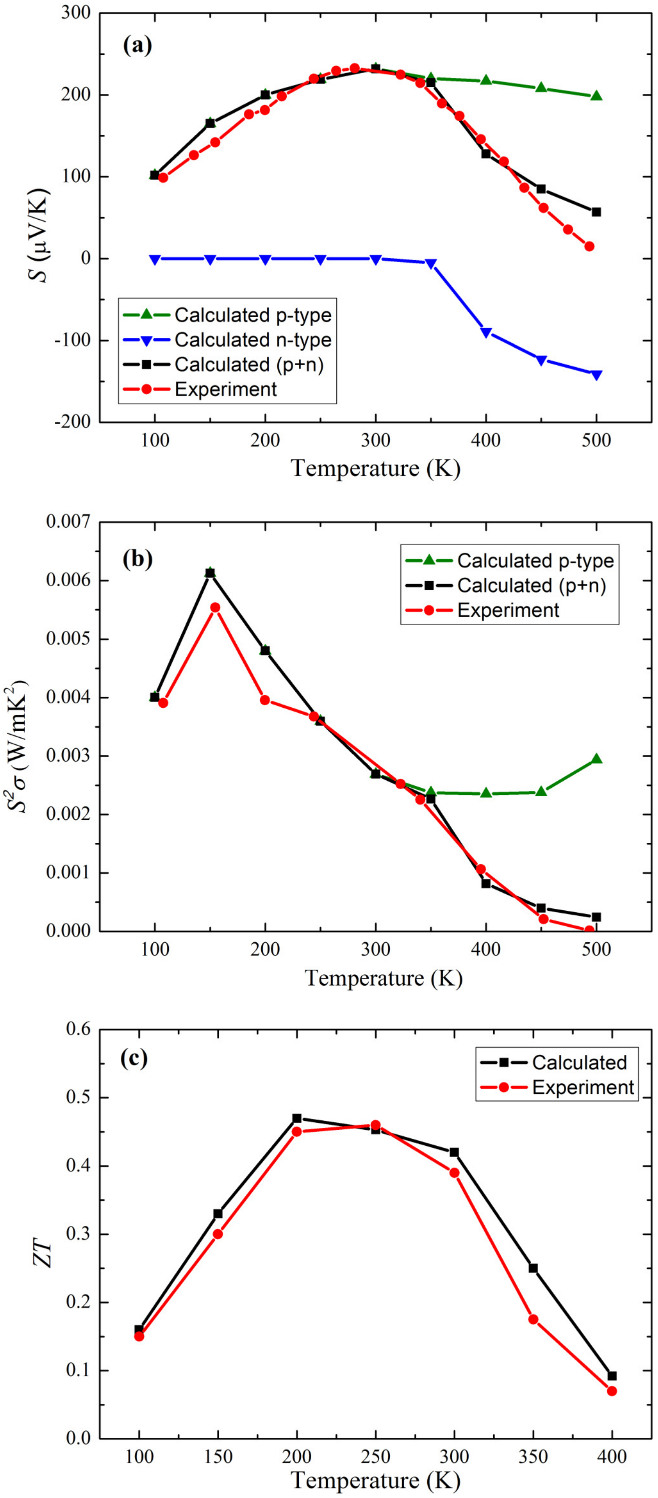

FIG. 4. (Color online) Calculated temperature dependence of (a) Seebeck coefficient, (b) power factor, and (c) *ZT* value of Bi_2Te_3 at the experimentally measured carrier concentration. The experimental data from Ref. [43] are also shown for comparison.

point, we have also calculated the Seebeck coefficients for n-type carriers. Indeed, we see from Fig. 4(a) that the n-type Seebeck coefficients are almost negligible below 300 K and the major carriers remain holes, but are comparable to those of p type at elevated temperature. If we consider both kinds of carriers, the calculated Seebeck coefficients agree well with the experimental results in the whole temperature range from 100 to 500 K. It is worth mentioning that the maximum Seebeck coefficient at 300 K we obtained is 323 μV/K, which is very close to the theoretical limit estimated previously (320 μV/K) [44].

The next transport coefficient we consider is the electrical conductivity. Within the Boltzmann theory, the electrical conductivity σ can only be calculated with respect to the relaxation time τ. In principle, the relaxation time can be obtained by fitting the experimentally measured electrical conductivity or resistivity [43]. Table III lists all the fitted results. At room temperature we see that the relaxation time is 1.06×10^{-14} s which is consistent with previously assumed values [45,47]. In Fig. 4(b) we plot the calculated power factors ($S^2\sigma$) of Bi_2Te_3 along the in-plane direction with respect to temperature. We see again that the calculated results match well with those measured experimentally below 300 K. If both the major and minor carriers are considered (especially at higher temperature), we find good agreement between our theoretical prediction and the experimental data.

For the calculations of electronic thermal conductivity κ_e, we use the Wiedemann-Franz law $\kappa_e = L\sigma T$, where σ is the electrical conductivity, T is the temperature, and L is the Lorentz number. For traditional metals, the Lorentz number is 2.45×10^{-8} V^2/K^2. However, for most semiconducting thermoelectric materials, it is lower than this value. Here we use a Lorentz number of 1.54×10^{-8} V^2/K^2 as determined previously for bulk Bi_2Te_3 [48,49]. With all the transport coefficients available, we can now evaluate the thermoelectric performance of Bi_2Te_3 by calculating the figure of merit, or $ZT = S^2\sigma T/(\kappa_e + \kappa_l)$. Note here the experimentally measured lattice thermal conductivity κ_l is inserted [43]. Figure 4(c) shows the calculated *ZT* value of Bi_2Te_3 along the in-plane direction as a function of temperature. The experimentally measured results [43] are also shown. We do not plot the data above 400 K since the corresponding lattice thermal conductivity measured in Ref. [43] is absent. In the whole temperature ranges considered, we see the calculated temperature dependence of *ZT* value exhibits very good agreement with that measured experimentally. The coincidence of our theoretical calculations with the experimental data emphasizes the importance and accuracy of vdW interactions and *GW* approximation in predicting the electronic and transport properties of Bi_2Te_3. The detailed comparison of our approach with other calculations can be found in the Supplemental Material [46].

IV. SUMMARY

In summary, we have demonstrated the important role of vdW interactions and quasiparticle corrections on the electronic and transport properties of Bi_2Te_3, which are usually ignored in the previous DFT calculations concerning its thermoelectric performance. We find that using the exchange correlation energy in the form of PBE and the vdW functional in the form of optB86b predicts the lattice parameters very close to the experimental values. However, such approach gives an energy band gap of 108 meV, which is still smaller than that measured experimentally. To address such underestimation, we perform the *GW* calculations on the band structure of Bi_2Te_3 and make a fine search in the whole Brillouin zone to locate the global VBM and CBM. The *GW* calculated band gap is 157 meV and matches the experimentally result very well. Moreover, using the *GW* calculations and Boltzmann theory, the temperature dependence of the Seebeck coefficients, the power factor, and the *ZT* value are derived and all of them well reproduce the experimental data. Our theoretical approach highlights the strong capability and necessity of considering both the vdW interactions and *GW* approximation in accurately predicting the thermoelectric transport properties of Bi_2Te_3 and other similar systems such as SnSe, black phosphorous, and transition-metal dichalcogenide.

ACKNOWLEDGMENTS

We thank financial support from the National Natural Science Foundation (Grants No. 51172167 and No. J1210061) and the “973 Program” of China (Grant No. 2013CB632502). We also acknowledge the financial support from the postgraduate programs under the “Fundamental Research Funds for the Central Universities” (Grant No. 2014202020206).

---

[1] X. Luo, M. B. Sullivan, and S. Y. Quek, Phys. Rev. B **86**, 184111 (2012).

[2] S. Grimme, J. Comp. Chem. **27**, 1787 (2006).

[3] M. Dion, H. Rydberg, E. Schröder, D. C. Langreth, and B. I. Lundqvist, Phys. Rev. Lett. **92**, 246401 (2004).

[4] J. Klimeš, D. R. Bowler, and A. Michaelides, Phys. Rev. B **83**, 195131 (2011).

[5] V. R. Cooper, Phys. Rev. B **81**, 161104 (2010).

[6] W. L. Liu, X. Y. Peng, X. L. Wei, H. Yang, G. M. Stocks, and J. X. Zhong, Phys. Rev. B **87**, 205315 (2013).

[7] H. Zhang, C. X. Liu, X. L. Qi, X. Dai, Z. Fang, and S. C. Zhang, Nat. Phys. **5**, 438 (2009).

[8] S. V. Eremeev, Y. M. Koroteev, and E. V. Chulkov, JETP. Lett. **91**, 387 (2010).

[9] S. V. Eremeev, G. Landolt, T. V. Menshchikova, B. Slomski, Y. M. Koroteev, Z. S. Aliev, M. B. Babanly, J. Henk, A. Ernst, L. Patthey, A. Eich, A. A. Khajetoorians, J. Hagemeister, O. Pietzsch, J. Wiebe, R. Wiesendanger, P. M. Echenique, S. S. Tsirkin, I. R. Amiraslanov, J. H. Dil, and E. V. Chulkov, Nat. Commun. **3**, 635 (2012).

[10] L. Hedin and S. Lundqvist, Solid State Physics **23**, 1 (1970).

[11] M. S. Hybertsen and S. G. Louie, Phys. Rev. B **34**, 5390 (1986).

[12] E. Kioupakis, M. L. Tiago, and S. G. Louie, Phys. Rev. B **82**, 245203 (2010).

[13] O. V. Yazyev, E. Kioupakis, J. E. Moore, and S. G. Louie, Phys. Rev. B **85**, 161101 (2012).

[14] I. A. Nechaev and E. V. Chulkov, Phys. Rev. B **88**, 165135 (2013).

[15] I. Aguilera, C. Friedrich, and S. Blugel, Phys. Rev. B **88**, 165136 (2013).

[16] Y. L. Chen, J. G. Analytis, J. H. Chu, Z. K. Liu, S. K. Mo, X. L. Qi, H. J. Zhang, D. H. Lu, X. Dai, Z. Fang, S. C. Zhang, I. R. Fisher, Z. Hussain, and Z. X. Shen, Science **325**, 178 (2009).

[17] P. E. Blöchl, Phys. Rev. B **50**, 17953 (1994).

[18] G. Kresse and J. Joubert, Phys. Rev. B **59**, 1758 (1999).

[19] G. Kresse and J. Hafner, Phys. Rev. B **47**, 558(R) (1993).

[20] G. Kresse and J. Hafner, Phys. Rev. B **49**, 14251 (1994).

[21] G. Kresse and J. Furthmüller, Comput. Mater. Sci. **6**, 15 (1996).

[22] J. P. Perdew, K. Burke, and M. Ernzerhof, Phys. Rev. Lett. **77**, 3865 (1996).

[23] J. Hafner, J. Comput. Chem. **29**, 2044 (2008).

[24] N. Marzari and D. Vanderbilt, Phys. Rev. B **56**, 12847 (1997).

[25] I. Souza, N. Marzari, and D. Vanderbilt, Phys. Rev. B **65**, 035109 (2001).

[26] A. A. Mostofi, J. R. Yates, Y. S. Lee, I. Souza, D. Vanderbilt, and N. Marzari, Comput. Phys. Commun. **178**, 685 (2008).

[27] G. Pizzi, D. Volja, B. Kozinsky, M. Fornari, and N. Marzari, Comput. Phys. Commun. **185**, 422 (2014).

[28] S. Nakajima, J. Phys. Chem. Solids **24**, 479 (1963).

[29] S. K. Mishra, S. Satpathy, and O. Jepsen, J. Phys.: Condens. Matter **9**, 461 (1997).

[30] P. Larson, S. D. Mahanti, and M. G. Kanatzidis, Phys. Rev. B **61**, 8162 (2000).

[31] P. Larson, V. A. Greanya, W. C. Tonjes, R. Liu, S. D. Mahanti, and C. G. Olson, Phys. Rev. B **65**, 085108 (2002).

[32] G. F. Wang and T. Cagin, Phys. Rev. B **76**, 075201 (2007).

[33] S. M. Young, S. Chowdhury, E. J. Walter, E. J. Mele, C. L. Kane, and A. M. Rappe, Phys. Rev. B **84**, 085106 (2011).

[34] W. Zhang, R. Yu, H.-J. Zhang, X. Dai, and Z. Fang, New J. Phys. **12**, 065013 (2010).

[35] J. Klimeš, D. R. Bowler, and A. Michaelides, J. Phys.: Condens. Matter **22**, 022201 (2010).

[36] K. Lee, E. D. Murray, L. Kong, B. I. Lundqvist, and D. C. Langreth, Phys. Rev. B **82**, 081101 (2010).

[37] I. G. Austin, Proc. Phys. Soc. London **72**, 545 (1958).

[38] C. Y. Li, A. L. Ruoff, and C. W. Spencer, J. Appl. Phys. **32**, 1733 (1961).

[39] G. A. Thomas, D. H. Rapkine, R. B. Van Dover, L. F. Mattheiss, W. A. Sunder, L. F. Schneemeyer, and J. V. Waszczak, Phys. Rev. B **46**, 1553 (1992).

[40] S. J. Youn and A. J. Freeman, Phys. Rev. B **63**, 085112 (2001).

[41] M. Kim, A. J. Freeman, and C. B. Geller, Phys. Rev. B **72**, 035205 (2005).

[42] P. Larson, Phys. Rev. B **68**, 155121 (2003).

[43] H. W. Jeon, H. P. Ha, D. B. Hyun, and J. D. Shim, J. Phys. Chem. Solids **52**, 579 (1991).

[44] B. L. Huang and M. Kaviany, Phys. Rev. B **77**, 125209 (2008).

[45] T. J. Scheidemantel, C. Ambrosch-Draxl, T. Thonhauser, J. V. Badding, and J. O. Sofo, Phys. Rev. B **68**, 125210 (2003).

[46] See Supplemental Material at http://link.aps.org/supplemental/10.1103/PhysRevB.90.085118 for details.

[47] M. S. Park, J. H. Song, J. E. Medvedeva, M. Kim, I. G. Kim, and A. J. Freeman, Phys. Rev. B **81**, 155211 (2010).

[48] D. M. Rowe and C. M. Bhandari, *Moden Thermoelectric* (Reston Publishing, Reston, VA, 1983).

[49] W. S. Liu, Q. Y. Zhang, Y. C. Lan, S. Chen, X. Yan, Q. Zhang, H. Wang, D. Z. Wang, G. Chen, and Z. F. Ren, Adv. Energy Mater. **1**, 577 (2011).